Catalysis Today 148 (2009) 88–96

Contents lists available at ScienceDirect

Catalysis Today

journal homepage: www.elsevier.com/locate/cattod

The metal-incorporated mesoporous carbon with high performance in capture and degradation of volatile nitrosamines

Jing Yang, Fang Na Gu, Hong Ji Wang, Yu Zhou, Jia Yuan Yang, Zheng Ying Wu, Jian Hua Zhu *

Key Laboratory of Mesoscopic Chemistry of MOE, College of Chemistry and Chemical Engineering, Nanjing University, Nanjing 210093, China

ARTICLE INFO

Article history:
Available online 14 April 2009

Keywords:
Turnover form carbon
SBA-15 mesoporous silica
Fe
N-nitrosopyrrolidine
Environmental catalysis

ABSTRACT

A new attempt to make novel catalysts for environment protection is reported in this article. The mesoporous carbon with disordered structure is prepared using SBA-15 silica as the hard template and the P123 micelles colluded in the channel as the carbon precursor in one-pot synthesis. To develop the composite of metal-incorporated mesoporous carbon, the metal salt such as ferric sulfate is also utilized as the additive in the synthetic process, resulting in the disordered mesoporous carbon to contain metal species such as α-Fe. Compared with the order mesoporous carbon and the silica/carbon hybrid materials, the disordered mesoporous carbon possesses a good adsorption ability of volatile nitrosamines along with an excellent catalytic activity in the degradation of nitrosamines.

1. Introduction

Degradation of carcinogenic pollutants is an important subject of environmental catalysis to protect public health. Among these pollutants nitrosamines are well-recognized teratogens and carcinogens in laboratorial animals and are considered potentially carcinogenic in humans. Nitrosamines are widespread in environment, from industrial workplace like rubber factory to tobacco smoke, and they can cause serious health risk even in trace amount. The health hazard caused by smoking cigarette has been well established. Nitrosamines in main stream smoke can directly deposit into the blood following inhalation through smoking, while environmental tobacco smoke (ETS) contaminates indoor air to injure the passive smokers. With the characteristic functional group of N–N=O in their structure [1], nitrosamines induce not only the cancers of lungs, but also the diseases of the larynx, oral cavity and pharynx [2], pancreas, kidneys and bladder. Although the quantity of nitrosamines in cigarette smoke, alcoholic beverages and certain foods are minute, their cumulative effect over several years can play a role in cancer. For instance, the ethanol with 40 ppm *N*-nitrosopyrrolidine (NPYR) caused a 5.5 fold increase in lung tumor multiplicity [3]. Volatile nitrosamines also remain in the exhaust gas and wastewater of chemical or rubber factory, associating with high risk of public health [4–7]. Approximately 60–90% of human cancers are attributed to environment factors, particularly the chemical carcinogens therefore controlling the nitrosamines pollution is of growing interest.

A lot of porous materials has been employed to remove nitrosamines in gas stream and solution [8–15], and among them zeolite exhibits a high activity in selective adsorption and catalytic degradation of nitrosamines [16–20]. Zeolite can capture the volatile nitrosamines among the hundreds compounds in tobacco smoke and then catalytically degrade the carcinogenic agents to non-carcinogenic fragments. Due to the inherent drawback of micropore, however, zeolite usually provokes large pressure drop in some actual applications such as aeration system, therefore mesoporous materials become the candidate because their wider channel system can overcome the size constraint of zeolite pores. In the experiments of eliminating nitrosamines in cigarette smoke [9], SBA-15 has shown a higher activity than zeolite NaY to degrade the bulky tobacco specific nitrosamines (TSNA) since the pore size of SBA-15 allows the whole pore system to be used while zeolitic pore is inaccessible. Nonetheless, these siliceous materials suffer from the lack of metal cations because of their inherent compositions, making against for the adsorption of nitrosamines since the metal cations are necessary to provide the electrostatic affinity towards nitrosamines. Consequently, various metal compounds have been introduced into the porous host as the modifier to conquer this problem [21–25], and these modifications assuredly result in some new composites with high performance. At the same time, a lot of attention has been paid on the adjusting surface curvature of pore wall in mesoporous materials, in order to elevate the efficiency of the composites in adsorption and catalysis through modulating the geometric microenvironment of active sites [26,27]. Xu et al. recently reported an attempt to create a suitable curvature or defects in channels of MCM-41, because these artificial defects were beneficial to accommodate the incorporated active components and to form high active site for capturing

* Corresponding author. Tel.: +86 25 83595848; fax: +86 25 83317761.
E-mail address: jhzhu@netra.nju.edu.cn (J.H. Zhu).

0920-5861/$ – see front matter © 2009 Elsevier B.V. All rights reserved.
doi:10.1016/j.cattod.2009.03.014

volatile nitrosamines in gas stream [28]. Since these defects of the pore wall were not ordered, this result disclosed the important contribution of these partly non-ordered structures in the adsorption of volatile nitrosamines. This gives us a valuable clue for the design and preparation of new adsorbents because it reveals the synergistic promotion on the performance of the porous composite by both the guest modifier and the surface curvature of host. Consulting the excellent adsorptive properties and the wide application of activated carbon [29], we try to combine the advantages of both mesoporous silica and porous carbon to develop the new catalysts with mesoporous structure and the carbon-covered surface.

Nanostructured carbon materials such as carbon nanotubes [30,31] attract rapidly growing attention due to the new possibilities for hydrogen storage in addition to the common applications as adsorbents [32,33], catalyst supports [34,35] and electrode materials [36]. Ryoo et al. [37] firstly reported the synthesis of mesoscopically ordered carbon designated as CMK-1 by carbonizing sucrose inside the pores of MCM-48 mesoporous silica. Since then most researches were focused on the carbon materials with the ordered structure. In general the synthesis of nanostructured carbon material contains two steps. Mesoporous silica is synthesized in the first step and then it is calcined to remove the original micelles occluded in channel because the silica will be used as a hard template. The second step is to introduce the carbon precursor into the empty channel, followed by the carbonization of the precursor and the removal of the mesoporous silica template with HF or NaOH solution [37,38]. When care is taken to elevate the atomic utilization of raw materials in synthesis, the removal of the template micelles inside the mesoporous silica, in our opinion, is the tremendous waste indeed, because the template micelle is the hydrocarbon that should be utilized as a kind of carbon precursor to prepare the mesoporous carbon. Accordingly, we plan to use the micelle as the carbon precursor to form a composite with a layer of carbon coating on the pore wall of the porous material, not only saving time and energy, but also reducing the cost of resulting functional materials. No doubt using the original template micelle as the only carbon precursor will induce the deficiency of carbon source, and it is impossible to replicate the structural symmetry of mesoporous silica. However, the resulting carbon materials with disordered structure can provide us a valuable chance to assess their actual performance in capturing and catalytically decomposing volatile nitrosamines, exploring the influence of surface curvature instead of the integral structural symmetry on the adsorption and catalytic performance. Some metal salts were introduced in the synthetic procedure to examine the influence of incorporated metal species on the performance of the resulting composite. On the other hand, the silica hard template would be preserved in some samples in order to check whether the mesoporous silica has promotion on the adsorption/catalysis of the hybrid materials. The instantaneous adsorption and temperature programmed surface reaction (TPSR) of *N*-nitrosopyrrolidine (NPYR) were employed to assess the actual function of the carbon materials in capture and degradation of volatile nitrosamines. NPYR is a typical volatile nitrosamine with a structure of five-member ring, and the adsorption and degradation of NPYR by zeolite or mesoporous silica have been extensively investigated [9,11,2,17,18]. Therefore, it is feasible to compare the performance of the disordered mesoporous materials with the ordered ones by using NPYR as the probe, in order to develop new carbon-containing porous catalytic materials for environment protection.

2. Experimental

N-Nitrosopyrrolidine (NPYR) was purchased from Sigma and dissolved in dichloromethane (A.R.) at the ratio of 1:19 (V/V). Tetraethylorthosilicate (TEOS) and P123 ($EO_{20}PO_{70}EO_{20}$) were the products of Shanghai Wulian (China) and Aldrich, respectively. Other regents with the AR purity were used as received.

Mesoporous silica SBA-15 was prepared according to literature [39]. In a typical synthesis of portion metal-carbon, 2.00 g P123, 30 g HCl (2 mol L^{-1}) and 43 g water were mixed and then 2.92 g sulfuric acid and a given amount of sulfate salt were added under vigorous stirring. When P123 was dissolved, 4.25 g TEOS was added. The molar ratio of the metal and Si was 0.1, including the sulfate of iron, magnesium, calcium, nickel and copper, respectively. The mixture was stirred for 1d, and then was placed in an autoclave for 24 h at 373 K. After the mixture was taken out of autoclave and vaporized at 358 K, the product was heated at 373 K for 6 h and then to 433 K for another 6 h. The resulting dark brown material was carbonized under nitrogen atmosphere at 1073 K for 5 h to realize the complete carbonization of P123, and then the silica/carbon composite was treated by NaOH solution to remove the silica and get the portion metal-carbon designed as TFC-metal (turnover form carbon, Scheme 1). Through the similar synthetic procedure without metal salt additive, sample TFC was prepared.

To synthesize silica/carbon composite, 100 g as-synthesized SBA-15 and 0.23 g H_2SO_4 (98%) were mixed with 5 g H_2O, and the ferric salt with Fe/Si molar ratio of 0.1 was added, then the mixture was treated with ultrasonic wave. After the product was heated at 373 K for 6 h then to 433 K for another 6 h, the resulting dark brown material was carbonized under nitrogen atmosphere at 1073 K for 5 h to get the silica/carbon composite Fe-C/SBA-15. Through the same synthetic procedure without metal salt additive, sample C/SBA-15 was prepared. CMK-3 was synthesized according to literature [40].

To characterize the samples, X-ray diffraction (XRD) patterns were recorded on an ARL XTRA diffractometer in the 2θ range of 0.5–90°. The Brunauer–Emmett–Teller (BET) specific surface area of sample was calculated using 77 K nitrogen adsorption data in the relative pressure range from 0.04 to 0.2, and the total pore volume was determined from the amount adsorbed at a relative pressure of about 0.99. The pore size distribution (PSDs) curves were calculated from the analysis of the desorption branch of the isotherm, using the Barret–Joyner–Halenda (BJH) algorithm. The scanning electron micrographs (SEM) were taken on a scanning electron microscope (SEM, LEO 1530 VP, Germany). The samples were coated with Au film to improve the conductivity prior to imaging. TEM analysis was performed on a FEI Tecnai G2 20 S-TWIN electron microscope operating at 200 kV. The metal contents of the TFC-Metal samples were measured by use of VARI AN AA240FS Fast sequential atomic absorption spectrometry.

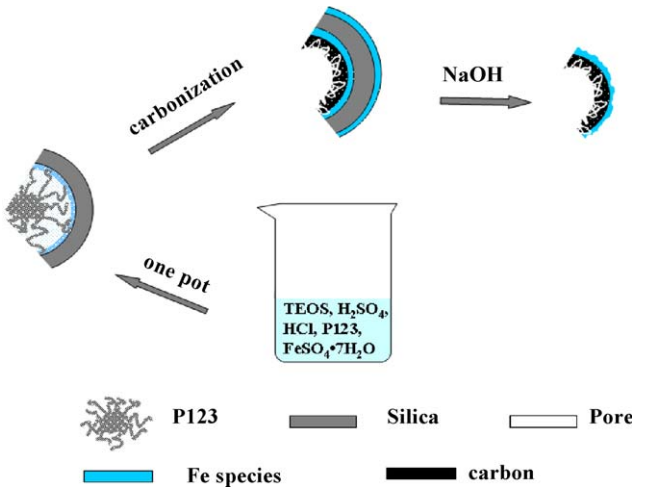

Scheme 1. Schematic diagram of the formation mechanism of TFC-Fe composite.

Instantaneous adsorption of volatile nitrosamines was carried out by use of gas chromatography (GC) method [17]. 5 mg sample (20–40 meshes) was filled in a stainless steel micro-reactor, with a 3 mm diameter and a 150 mm length, whose one end inserted deeply into the injector port of Varian 3380 GC and another end connected with the separation column (10% Carbowax 20 M +5% KOH with a 3 mm diameter and a 3000 mm length) in the GC. The sample was directly heated to the given temperature without activation, in the flow of carrier gas with a rate of 30 ml min^{-1} and the solution of nitrosamine was pulse injected with the amount of 2 (L each time. Thermal conductivity detector of GC was used to analyze the gaseous effluent, and the decrement in the ratio of solute to solvent was utilized to calculate the adsorbed amount [12,27].

A TPSR (temperature-programmed surface reaction) test was employed to assess the degradation of nitrosamines on metal-carbon materials. A certain mass of sample (20–40 meshes) was first activated at 773 K in the nitrogen gas flow with the rate of 30 mL min^{-1} for 2 h, and then cooled to 313 K to contact 100 μL of dichloromethane solution of NPYR. After the sample was purged to remove the physically adsorbed NPYR, the temperature was raised to 773 K at the rate of 10 K min^{-1} while the nitrogen oxide products formed in the decomposition of nitrosamines were detected by an advanced photometric method [10]. The amount of NO_x determined in the TPSR procedure represents the amount of nitrosamines decomposed on the metal-carbon materials [18].

3. Results and discussion

3.1. Structure property of carbon-containing mesoporous materials

Fig. 1 displays the wide-angle XRD patterns of TFC-Fe sample. There were two different crystalline phases in the composite of TFC-Fe, i.e. cubic (JCPDS card 85-1410) and hexagonal-close-packing (hcp) designed epsilon-iron (JCPDS card 34-0529) phases. It is known that the bcc phase grows with the (1 1 0), while the hcp phase is textured with the (1 0 1) preferential orientation [41]. Thus, the peaks with 2θ value of 44.6°, 64.8° and 82.0° corresponded to the (1 1 0), (2 0 0) and (2 1 1) crystal plane of α-Fe with body center cubic (bcc) structure; another two peaks with the 2θ value of 20.7° and 22.5° originated from ε-Fe with the hcp structure. Existence of two phases of metal iron in the composite indicated the reduction of ferric salt during the carbonization process. Fe-C/SBA-15 sample also possessed the XRD peaks of Fe in the wide-angle patterns as presented in Fig. 1, there was one weak characteristic of ε-Fe at 2θ of 22.4° whereas several unremarkable peaks of Fe_2O_3 emerged at

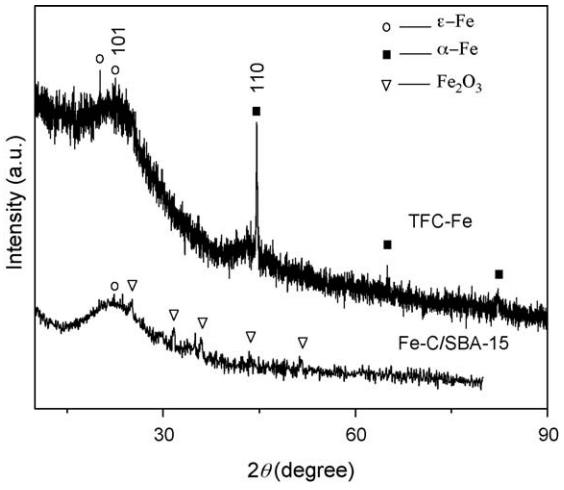

Fig. 1. The Wide-angle XRD patterns of TFC-Fe and Fe–C/SBA-15 samples.

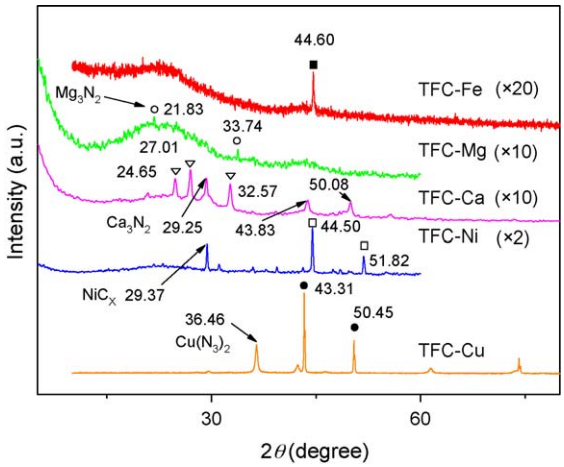

Fig. 2. The Wide-angle XRD patterns of TFC-Metal samples.

23.7°, 31.7°, 34.9°, 43.4° and 51.4° (2θ value), respectively. In addition, there was a broad peak of amorphous silica on the patterns as expected. Based on these XRD analysis results, it appears that ultrasonic treatment is beneficial to disperse the ferric salt in SBA-15, whilst part of the ferric guest is oxidized to Fe_2O_3 due to the high dispersion on and the interaction with the mesoporous silica host.

Fig. 2 presents the wide XRD patterns of TFC-Metal samples. TFC-Mg did not have the magnesium metal phase in its XRD patterns, the diffraction peaks with 2θ value of 21.83° and 33.74° were appointed to those of Mg_3N_2 (JCPDS card 73-1070). The characteristic of nitride (JCPDS card 22-0152 of Ca_3N_2) emerged on the XRD patterns of TFC-Ca sample, accompanied with several peaks of metal Ca that emerged at 24.64°, 27.01° and 32.57° (2θ value). After the nickel sulfate was introduced into the TFC-Ni sample, many characteristic peaks of the guest appeared on the XRD pattern. The peak at 29.25° was attributed to NiC_x, and those at 44.5° and 51.82° assigned to metal Ni. For the TFC-Cu sample, the sharp peaks around 43.31° and 50.45° were the characteristic (1 1 1) and (2 0 0) diffractions of copper (JCPDS card 85-1326), another peak at 36.46° was the feature of $Cu(N_3)_2$.

Fig. 3A illustrates the low-angle XRD patterns of TFC and TFC-Fe samples. Both composites had only one diffraction peak (0 0 1) reflection that corresponds to a basal spacing of 8.8 nm, yet their featureless XRD patterns meant a low degree of long-range pore ordering. The absence of additional reflections meant a distorted structure and lattice shrinkage rationally occurring in the 2D hexaganal packing carbon nanorods with the little interconnection after silica removal [42–44]. Introducing Fe into TFC caused a weaker ordered meso-structure in the resulting composite in comparison with TFC itself, indicating the influence of cation on the mesostucture due to the salting-out or salting-in nature of the cation [45,46]. Fig. 3B displays the low-angle XRD patterns of Fe-C/SBA-15 and C/SBA-15, where the (1 0 0), (1 1 0) and (2 0 0) reflections from hexagonal structures are similar to those of SBA-15 [39]. This similarity confirms the long-range ordering of these silica/carbon composites. Fig. 3B also shows the pattern of ordered carbon CMK-3 with the well-resolved low-angle XRD peaks that are assigned to (1 0 0), (1 1 0), and (2 0 0) diffractions of the 2D hexagonal space group (*p6mm*), similar to that of SBA-15. On the basis of these results, it is very likely that using template micelles as carbon resource plus removing silica framework from the resulting composite can only form the disordered mesoporous materials no matter whether they contain the guest metal species or not.

Fig. 4A demonstrates the N_2 adsorption–desorption isotherms of TFC, TFC-Fe and CMK-3 composites. The isotherms of TFC and TFC-Fe exhibited the characteristic isotherms resembling type IV via

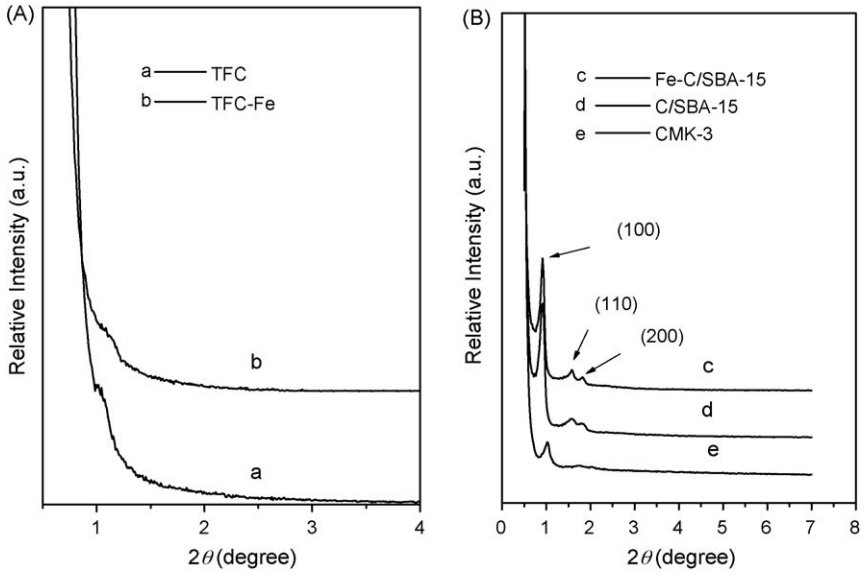

Fig. 3. Low-angle XRD patterns of (a) TFC and (b) TFC-Fe, (c) Fe–C/SBA-15, (d) C/SBA-15, and (e) CMK-3 samples.

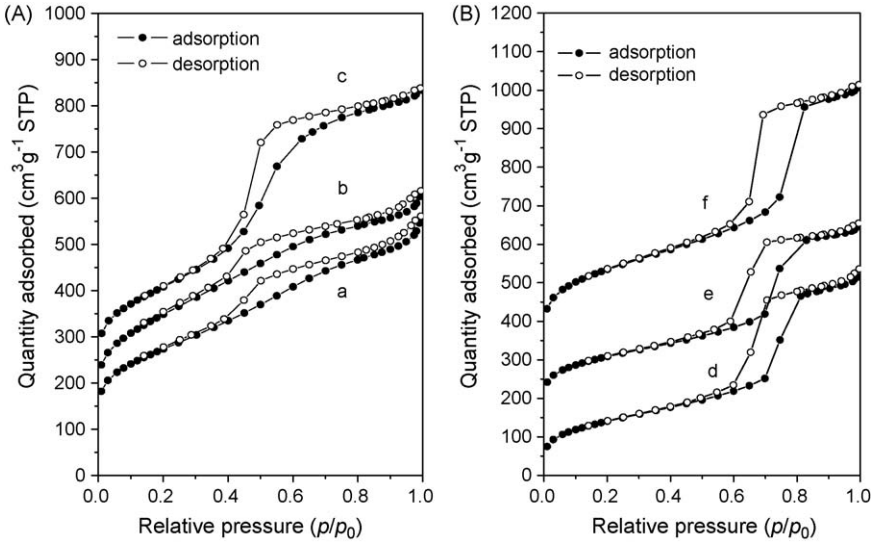

Fig. 4. N_2 adsorption–desorption isotherms of (a) TFC-Fe, (b) TFC, (c) CMK-3, (d) Fe–C/SBA-15, (e) C/SBA-15, (f) SBA-15 (the isotherms for b, c, e and f are offset vertically by 50, 100, 150 and 300 $cm^3\ g^{-1}$, respectively) at 77 K.

multilayer adsorption followed by capillary condensation, and their hysteresis loops possessed a combination of H2 and H4 [47]. CMK-3 had a hysteresis loop with the character of type-H1 at p/p_0 between 0.4 and 1, different from the two disordered materials TFC and TFC-Fe. Clearly in this case, insufficient carbon source of TFC and TFC-Fe resulted in the characteristic of ink-bottle pores and slit-like pores structure during the carbonized process. Fig. 4B depicts the isotherms of C/SBA-15 and Fe-C/SBA-15; both of them were type IV with a clear type-H1 hysteresis loop at high relative pressure that were typical of mesoporous materials with 1D cylindrical channels, and the curves were quite similar to that of the parent SBA-15. However, the onset of the inflections slightly shifted toward lower p/p_0 values, and the adsorption amount of N_2 decreased owing to the incorporation of guest species in SBA-15. As shown in Table 1, the surface area of two samples also decreased gradually with the introduction of carbon and iron. Fe-C/SBA-15 had a smaller micropore area than C/SBA-15 or SBA-15, due to the insertion of guest into the small pore, but its an average pore diameter of 6.09 nm was larger than C/SBA-15 (5.25 nm) and SBA-15 (5.08 nm). This difference resulted from the effect of inorganic salt additive in the synthesis of SBA-15, since these salts made the silica wall ultimately thinner hence the pore size became slightly larger [48].

Fig. 5 depicts the N_2 adsorption–desorption isotherms of TFC-Metal samples. All of these metal-containing composites had the

Table 1
The textual properties of SBA-15 and carbon samples.

Sample	S_{BET} ($m^2\ g^{-1}$)	V_p ($cm^3\ g^{-1}$)	S_{mic}[a] ($m^2\ g^{-1}$)	V_{mic} ($cm^3\ g^{-1}$)	d_{BJH}[b] (nm)
TFC	1067	0.82	166	0.07	3.08
TFC-Fe	967	0.81	241	0.11	3.33
TFC-Cu	527	0.45	158	0.07	3.44
TFC-Mg	855	0.57	263	0.12	2.66
TFC-Ni	859	0.76	193	0.08	3.52
TFC-Ca	672	0.53	165	0.07	3.16
CMK-3	1072	1.12	255	0.11	4.10
SBA-15	846	1.07	137	0.05	5.08
C/SBA-15	570	0.75	95	0.04	5.25
Fe-C/SBA-15	511	0.78	33	0.01	6.09

[a] Micropore area.
[b] BJH average pore diameter.

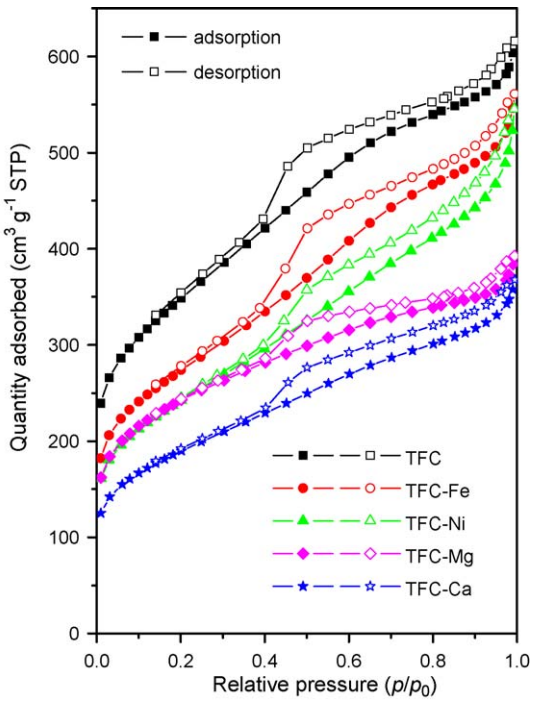

Fig. 5. The N_2 adsorption–desorption isotherms of TFC-Metal samples at 77 K.

sorption isotherms of type IV along with a sharp capillary condensation step indicative of mesopores narrowly distributed in size. Table 1 summarizes the structural and textural properties of these samples. Introduction of metal species in the turnover form carbon changed the textural property of resulting composites, decreasing the surface areas from 1067 $m^2\ g^{-1}$ (TFC) to the minimum of 527 $m^2\ g^{-1}$ (TFC-Cu), while the pore volume declined from 0.82 to 0.45 $cm^3\ g^{-1}$.

Fig. 6 exhibits the SEM images of TFC and TFC-Fe composites. The former looked like micrometer-sized rods and the latter was the fiber bundles, both of them were different from the morphology of SBA-15 rod that was plump and rounded [39]. The deficiency of the carbon precursor in TFC and TFC-Fe samples made them fail to replicate the structure and morphology of SBA-15 therefore only disordered porous materials was produced. Fig. 7 shows the TEM images of TFC and TFC-Fe samples to reveal their morphology and microstructure. There was a wormhole-like framework in TFC composite, and a majority of it was the disordered structure, coincided with the low-angle XRD results. After incorporating ferric species into the TFC composite, the morphology of TFC-Fe varied obviously. The strong contrast between the dark core and the relatively bright edge was the evidence for the real high dispersion of Fe species on TFC sample.

3.2. Adsorption of NPYR in gas stream by carbon-containing composites

Instantaneous adsorption method provides a quick technique to evaluate the capability of porous material in adsorption of volatile nitrosamines in gas flow [17]. Fig. 8 illustrates the adsorption of NPYR by carbon-based composite at 453 K. Among the five samples, CMK-3 exhibited the highest ability to capture NPYR in gas stream and its adsorption capacity kept increasing in the experiment, whereas SBA-15 had the lowest ability. When 1.0 mmol g^{-1} of NPYR passed through the samples, SBA-15 adsorbed 15%, C/SBA-15 trapped 24%, Fe-C/SBA-15 captured 52%, while TFC-Fe and CMK-3 adsorbed 56% and 68%, respectively. In order to deeply inspect the role played by the ordering of mesopores in the instantaneous adsorption of volatile nitrosamines such as NPYR, sample TFC was utilized to perform this adsorption and to be compared with CMK-3. However, the adsorptive capacity of TFC sample (34%) was obviously inferior to that of CMK-3 (68%) under the same accumulated amount of NPYR (1.0 mmol g^{-1}), although two carbon samples had the almost

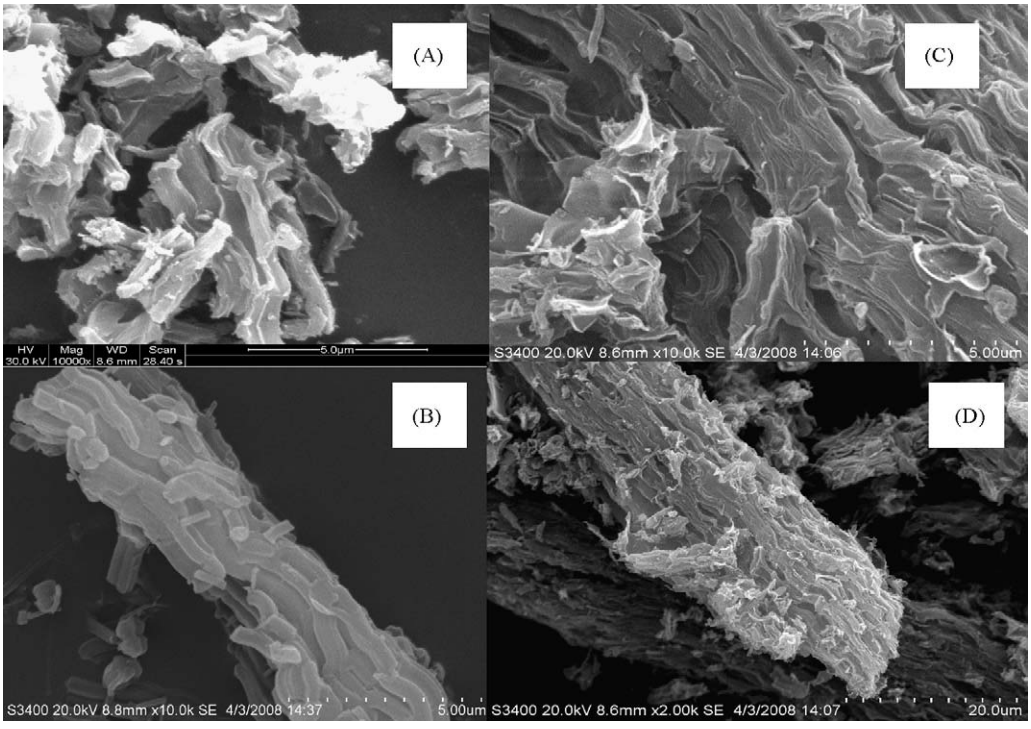

Fig. 6. SEM images of (A) TFC, (B) SBA-15 and (C, D) TFC-Fe composites.

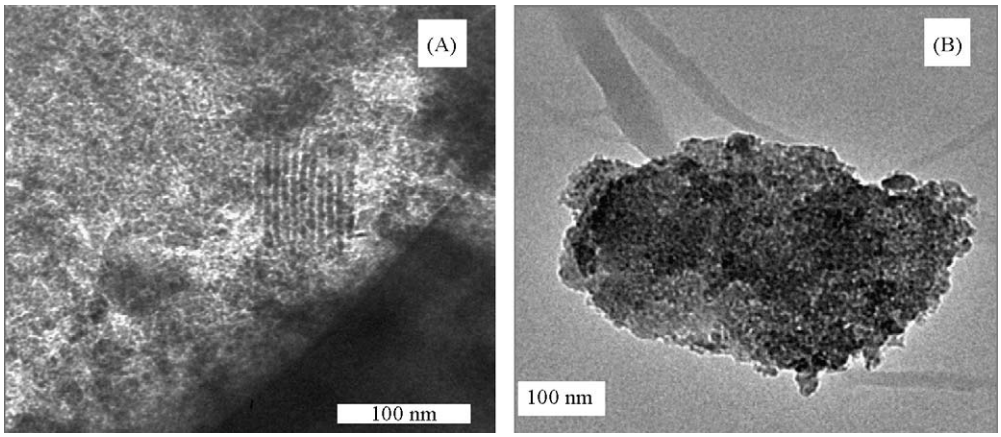

Fig. 7. TEM images of (A) TFC and (B) TFC-Fe composites.

same surface area (Table 1). Also, CMK-3 exhibited a superior adsorptive ability to TFC throughout the total test process as demonstrated in Fig. 8. Two factors should be taken into account for this difference. The first is the different structure of two adsorbents, CMK-3 had the mesoporous structure more regular than TFC sample as demonstrated in the low-angle XRD patterns; the second is the different proportion of micropores in two samples, because the micro surface area of CMK-3 (255 $m^2 g^{-1}$) was obviously larger than that of TFC (166 $m^2 g^{-1}$). Judged from these differences, it is clear that both ordered mesoporous structure and the suitable microporous environment are beneficial for the porous carbon to capture the volatile nitrosamines such as NPYR in gas stream.

To accurately assess the adsorptive ability of the samples and to exclude the influence of their surface area, we calculate the adsorption capacity of every sample by $\mu mol\ m^{-2}$ instead of $mmol\ g^{-1}$. As a result, the calculated adsorptive ability of SBA-15, C/SBA-15 and Fe-C/SBA-15 was 0.18, 0.42 and 1.02 $\mu mol\ m^{-2}$, and the corresponding value of TFC, TFC-Fe and CMK-3 was 0.36, 0.58 and 0.63 $\mu mol\ m^{-2}$, respectively. Based on these results, it is clear that coating a layer of disordered carbon on the pore wall of SBA-15 can change the surface property more or less, and thus promotes the adsorption of volatile nitrosamines in gas stream. Likewise, incorporation of ferric species in the carbon/silica composite further improves the adsorptive ability. In the instantaneous adsorption process of volatile nitrosamines, the contact time between adsorbent and adsorbate is shorter than 0.1 s [17], therefore the porous adsorbent should possess the suitable geometric micro-environment to confine the movement of the target and to enlarge the collide frequency between the target and the adsorptive site. Besides, powerful active site is crucial for the adsorption to hold the target molecules. For volatile nitrosamines such as NPYR, electrostatic interaction from the cation of adsorbent toward the functional group of N–NO in nitrosamines is necessary [12,17,27,28], which will induce the whole nitrosamine molecule to move into the channel of adsorbent. Accordingly, coating a layer of disordered carbon onto the channel wall of SBA-15 can tailor the curvature and defects of the wall, enhancing the frequency of collide of NPYR within the channel so that the target is more easily trapped by the composite. Likewise, introduction of ferric species in the composite brings more cations hence the electrostatic interaction is strengthened [13]. From the comparison between SBA-15 and CMK-3 with the similar structural symmetry, it is safe to conclude that carbon can be better to adsorb nitrosamines than silica although they are in similar structure, because SBA-15 adsorbed less NPYR (0.18 $\mu mol\ m^{-2}$) than CMK-3 (0.63 $\mu mol\ m^{-2}$). This may be the reason why activated carbon has been widely used in tobacco industry as the filter additive [49] or purifier of water [50]. Further confirmation on this inference came from the comparison between SBA-15 and C/SBA-15 in which the latter exhibited a considerable higher activity than the former. Nonetheless, amorphous activated carbon with a surface area of 921 $m^2 g^{-1}$ could trap more NPYR (0.71 $\mu mol\ m^{-2}$ [13]) than CMK-3 (0.63 $\mu mol\ m^{-2}$) under the same conditions, which might reflect the minor function of mesopore in the adsorption of volatile nitrosamines in gas stream by porous carbon materials, the inherent nature of carbon determined the adsorptive performance of amorphous activated carbon or mesoporous CMK-3. Comparing the performance of two mesoporous materials, SBA-15 and Fe-C/SBA-15, can give more information on the adsorption of NPYR. As aforementioned, the presence of carbon in mesoporous materials could favor the adsorption of volatile nitrosamines, and the existence of Fe dramatically promoted the adsorption ability of the composite. In general, the microporous pore in SBA-15 was believed to favor the capture of volatile nitrosamines [28]. However, Fe-C/SBA-15 captured more NPYR than SBA-15 under the same conditions whereas the microporous area of Fe-C/SBA-15 (33 $m^2 g^{-1}$, Table 1) was much smaller than that of SBA-15 (137 $m^2 g^{-1}$). The above studies demonstrate that introducing metal cation into mesoporous silica has a stronger influence on the adsorption of NPYR than that of micropore; in other words, the electrostatic interaction toward volatile nitrosamines plays a crucial role in the instantaneous adsorption.

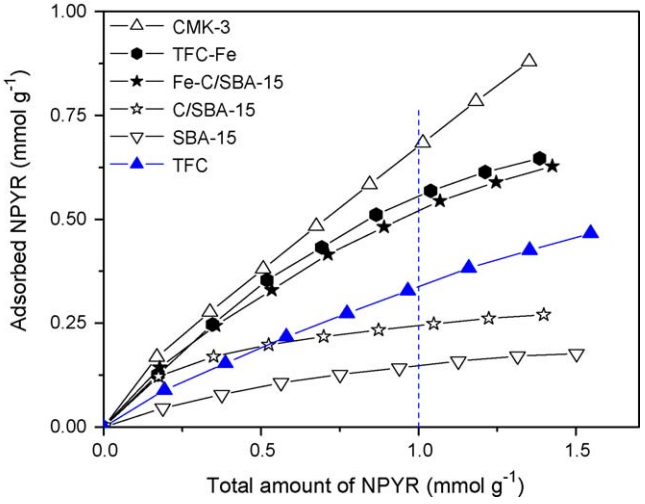

Fig. 8. Adsorption of NPYR on CMK-3, TFC-Fe, Fe–C/SBA-15, C/SBA-15 and SBA-15 at 453 K.

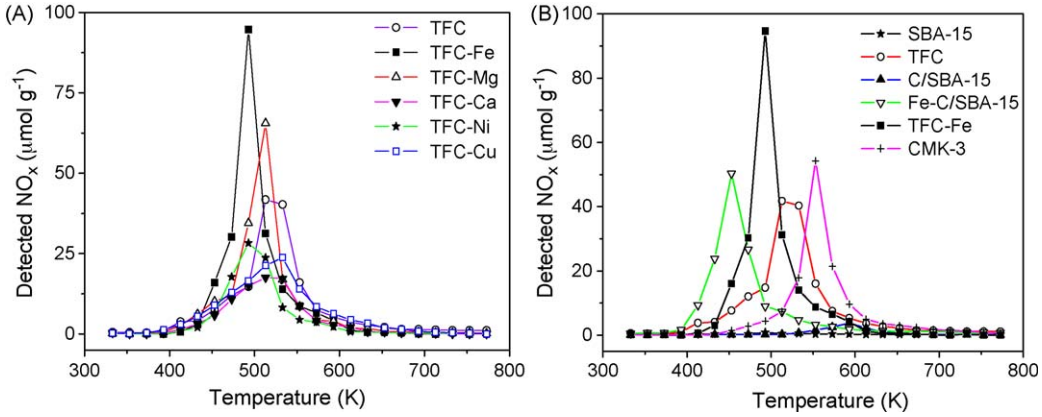

Fig. 9. Profiles of nitrogen oxide desorbed from (A) TFC and TFC containing metal and (B) SBA-15, TFC, C/SBA-15, Fe–C/SBA-15, TFC-Fe and CMK-3.

3.3. Catalytic degradation of NPYR by the carbon-containing composites

To evaluate the catalytic function of carbon-based composites for the degradation of volatile nitrosamines such as NPYR, temperature programmed surface reaction (TPSR) test was carried out and the detected amount of nitrogen oxides represented the amount of nitrosamines degraded in the thermal process [9,12,16]. Fig. 9A demonstrates the degradation of NPYR on a series of TFC-Metal materials via the increasing temperature, among them TFC-Fe composite exhibited the highest activity to degrade the volatile nitrosamines and the strong desorption peak of NO_x emerged in the profile of TFC-Fe around 493 K with an amount of 213 μmol g^{-1}. TFC-Mg sample showed an activity similar to that of TFC to decompose NPYR, producing the NO_x products (173 μmol g^{-1}) similar to that of TFC (171 μmol g^{-1}), and their climaxes of NO_x desorption appeared around 513 K on the profile (Table 2). The least amount of nitrogen oxides, 92 μmol g^{-1}, was collected on TFC-Ca sample, while TFC-Ni and TFC-Cu displayed a smaller desorption of NO_x than TFC itself. These phenomena mirror the influence of metal guest on the decomposition of nitrosamines, involving the dispersion and distribution of the guest along with the guest-host interaction. Table 2 lists the data of metal content in those TFC-Metal samples accompanied with their corresponding theoretic value, in which the detected metal content differs from the calculated value more or less. Apart from the experimental error, another reason should be taken into account for this difference. In the experiment of carbonization, part of P123 decomposes to form other volatile compounds rather than carbon at relatively lower temperature, for instance during the carbonization at 373 K and 433 K. As a result, the weight of carbon formed is decreased and thus the metal content increases. On the other hand, the detected metal contents in the TFC-Metal composites varied in the range of 3–15%, and the crystalline phase peaks of the metal species emerged on the corresponding wide-angle XRD patterns (Figs. 1 and 2), it is easy to image that these metal guests may form multilayer on TFC host hence the dispersion and distribution of the metal guest will seriously affect the actual function of the composite. For instance TFC-Fe and TFC-Ni samples had similar metal contents, 9.0% and 9.1%, respectively, but their abilities in degradation of NPYR were quite different because the surface area of TFC-Fe was higher than that of TFC-Ni sample. That is to say, TFC-Fe enables the metal guest to be dispersed better and thus possesses more active sites to adsorb and degrade NPYR. Also, the nature of metal species affects the interaction with N–NO group of NPYR, accelerating the decomposition of NPYR. Nitrosamines are the carcinogens having the both weak acidity and weak basicity [10], while the ferric species also possessed an especial acidic-basic property; therefore the introduction of Fe or ferric compounds on porous composite would lead to a suitable chemical environment for trapping the carcinogens. At the same time, desorption of NO might become easier and thus happened at an obviously lower temperature. These advantages of ferric modification enable TFC-Fe to be highly active for the degradation of volatile nitrosamines, and the amount of NPYR degraded on TFC-Fe exceeds that on copper modified SBA-15 (72.4 μmol g^{-1}, [51]). Based on the results of the preliminary test, TFC-Fe composite was selected to perform the succeeding experiments.

Fig. 9B illustrates the comparison of disordered porous TFC materials with silica/carbon composite as well as mesoporous carbon CMK-3. The amount of NO_x products detected on TFC-Fe (213 μmol g^{-1}) was still the highest, while SBA-15 exhibited the lowest activity to decompose NPYR (Table 2). C/SBA-15 showed a higher activity than SBA-15, on the former, double amount of NO_x was captured (15 μmol g^{-1}), mirroring the promotion of carbon in the mesoporous silica on the degradation of volatile nitrosamines.

Table 2
Catalytic performance of carbon and metal-carbon samples.

Samples	Total amount of NO_x (μmol g^{-1})	Total amount of NO_x (μmol m^{-2})	T_{max} (K)	Experimental metal content (wt.%)	Theoretic metal content (wt.%)
TFC	171	0.160	513	0	0
TFC-Fe	213	0.220	493	9.0	8.7
TFC-Cu	136	0.258	513	15.7	10.2
TFC-Mg	173	0.202	513	3.3	3.9
TFC-Ca	92	0.107	513	6.1	6.4
TFC-Ni	102	0.152	493	9.1	9.0
CMK-3	140	0.131	553	0	0
SBA-15	7	0.008	493	0	0
C/SBA-15	15	0.026	593	0	0
Fe–C/SBA-15	131	0.256	453	4.4	4.5

Fe-C/SBA-15 possessed a much higher activity than C/SBA-15 as expected, and this phenomenon indicated the obvious promotion of the Fe species in the composite on the degradation of NPYR. It is worthy to mention that the amount of NO_x products detected on TFC sample was slightly higher than that on CMK-3. Both TFC and CMK were mesoporous carbon materials with similar surface area (Table 1), yet TFC had a smaller pore volume than CMK-3. Moreover, CMK-3 had a fully ordered structure with the hexagonal pore arrangement whereas TFC possessed a disordered structure (Fig. 2A). The different catalytic activity between TFC and CMK-3 may mean that the ordered structure of mesoporous materials is not crucial for the degradation of volatile nitrosamines, similar to the "unimportance of regularity" for catalytic nanostructures [52]. Therefore, it is possible for the mesoporous materials with disordered structure to possess a higher activity in degrading NPYR. To get a deep inspection on the data of NPYR-TPSR experiments, we also calculate the catalytic performance of composite in unit area instead of unit weight, that is, to calculate the concentration of nitrogen oxides to $\mu mol\ m^{-2}$ instead of $\mu mol\ g^{-1}$. Accordingly, there was NO_x of 0.008 $\mu mol\ m^{-2}$ formed on SBA-15 and 0.026 $\mu mol\ m^{-2}$ on C/SBA-15. For Fe-C/SBA-15 sample, this value rose to 0.26 $\mu mol\ m^{-2}$. This increasing sequence indicates the importance of incorporating carbon and ferric species in mesoporous silica for the removal of volatile nitrosamines as aforementioned. That is to say, the surface properties of the support play an important role in the adsorption or catalysis. Likewise, the amount of NO_x products detected on TFC was 0.16 $\mu mol\ m^{-2}$, slightly higher than the value of CMK-3 (0.13 $\mu mol\ m^{-2}$), but lower than that of TFC-Fe (0.22 $\mu mol\ m^{-2}$), 2), confirming further the crucial function of metal component for the catalytic degradation of nitrosamines. On the other hand, the value of temperature T_{max}, at which the maximum value of nitrogen oxide products emerged, gives the further evidence on the different activity of these carbon-based porous catalysts. The value of T_{max} was in the decreasing order: T_{max} (Fe-C/SBA-15) < T_{max} (TFC-Fe) < T_{max} (TFC) < T_{max} (CMK-3) as demonstrated in Table 2. The degradation of volatile nitrosamines such as NPYR is known to begin from the cleavage of the N–N band in the functional group N–NO and to liberate the products of nitrogen oxides therefore the value of T_{max} reflects the activity of the catalyst [18], the lower value of T_{max}, the more active the catalyst. The higher activity of Fe-C/SBA-15, TFC-Fe and TFC samples than that of CMK-3 reveals the minor role played by the ordered pore structure in the catalytic decomposition of nitrosamines by carbon materials, and confirms the strategy of enhancing the activity of the carbon-based composite through incorporation of metal species for the potential application in environmental catalysis.

4. Conclusion

(1) Through utilizing the original template micelles as the carbon source, we successfully synthesized the series of TFC-Metal composites with disordered mesoporous structure and the ordered mesoporous carbon-coated SBA-15 hybrid materials. This new process was characterized with the advantage of time- and energy-saving.

(2) After the incorporation of ferric species, the modified composites with disordered or ordered mesoporous structure could exhibit a comparable activity with CMK-3, the typical mesoporous carbon, in the instantaneous adsorption and catalytic degradation of volatile nitrosamine NPYR. Besides, introducing carbon or ferric guest also promotes SBA-15 to capture NPYR in gas stream and to catalyze the degradation of NPYR, demonstrating the crucial role played by the surface properties of porous materials in these adsorption and catalysis processes.

(3) With the same composition of carbon, CMK-3 exhibits a higher capability than TFC in adsorption of volatile nitrosamines. This result indicates the important function of the ordered mesoporous structure in adsorption. On the other hand, the high activity of TFC and TFC-Fe composites in the catalytic degradation of NPYR demonstrates that the disordered pore structure is also beneficial for the catalytic elimination of volatile nitrosamines in environment.

This study is our first preliminary approach to demonstrate the performance characteristics of new hybrid composite with disordered structure for the capture and degradation of nitrosamines. Further comprehensive investigations are required to clearly identify detail the property-function characteristics of these new materials.

Acknowledgment

Financial support from NHTRDP973 (2007CB613301), NSF of China (20773601 and 20873059), Grant 2008AA06Z327 from the 863 Program of the Ministry of Science and Technology of China, the Scientific Research Foundation of Graduate School of Nanjing University, Grant CX08B_009 from Jiangsu Province Innovation for PhD candidate and Analysis Center of Nanjing University is gratefully acknowledged.

References

[1] H. Bartsch, H. Ohshima, B. Pignatelli, S. Camels, Cancer Surveys 8 (1989) 335.
[2] B. Prokopczyk, D. Hoffmann, M. Bologna, A.J. Cunningham, N. Trushin, S. Akerkar, T. Boyiri, S. Amin, D. Desai, S. Colosimo, B. Pittman, G. Leder, M. Ramadani, D. Henne-Bruns, H.G. Beger, K. El-Bayoumy, Chem. Res. Toxicol. 15 (2002) 677.
[3] L.M. Anderson, J.P. Carter, C.L. Driver, D.L. Logsdon, Cancer Lett. 68 (1993) 61.
[4] K. Straif, S. Weiland, B. Werner, A. Wienke, U. Leil, Am. J. Ind. Med. 35 (1999) 264.
[5] S. Monarca, D. Feretti, A. Zanardini, M. Moretti, M. Villarini, B. Spiegelhader, I. Zerbini, U. Gelatti, E. Lebbolo, Mutat. Res. 490 (2001) 159.
[6] W. Altkofer, S. Braune, K. Ellendt, M. Kettl-Grömminger, G. Steiner, Mol. Nutr. Food Res. 49 (2005) 235.
[7] J.O. Sharp, T.K. Wood, L. Alvarez-Cohen, Biotechnol. Bioeng. 89 (2005) 608.
[8] M.W. Meier, K. Siegmann, Microporous Mesoporous Mater. 33 (1999) 307.
[9] J.H. Zhu, S.L. Zhou, Y. Xu, Y. Cao, Y.L. Wei, Chem. Lett. 32 (2003) 338.
[10] Y. Xu, J.H. Zhu, L.L. Ma, A. Ji, Y.L. Wei, X.Y. Shang, Microporous Mesoporous Mater. 60 (2003) 125.
[11] Y. Wang, S.L. Zhou, J.R. Xia, J. Xue, J.H. Xu, J.H. Zhu, Microporous Mesoporous Mater. 75 (2004) 247.
[12] Y. Cao, L.Y. Shi, Z.Y. Yun, C.F. Zhou, Y. Wang, J.H. Zhu, Environ. Sci. Technol. 39 (2005) 7254.
[13] Y. Cao, L.Y. Shi, C.F. Zhou, T.T. Zhuang, Y. Wang, J.H. Zhu, Stud. Surf. Sci. Catal. 156 (2005) 595.
[14] J.H. Zhu, D. Yan, J.R. Xia, L.L. Ma, B. Shen, Chemosphere 44 (2001) 949.
[15] C.F. Zhou, J.H. Zhu, Chemosphere 58 (2005) 109.
[16] Y. Cao, Z.Y. Yun, J. Yang, X. Dong, C.F. Zhou, T.T. Zhuang, Q. Yu, H.D. Liu, J.H. Zhu, Microporous Mesoporous Mater. 103 (2007) 352.
[17] C.F. Zhou, Y. Cao, T.T. Zhuang, W. Huang, J.H. Zhu, J. Phys. Chem. C 111 (2007) 4347.
[18] Z.Y. Wu, H.J. Wang, L.L. Ma, J. Xue, J.H. Zhu, Microporous Mesoporous Mater. 109 (2008) 436.
[19] L. Gao, Y. Wang, Y. Xu, S.L. Zhou, T.T. Zhuang, Z.Y. Wu, J.H. Zhu, Clean: Soil, Air Water 36 (2008) 270.
[20] J. Yang, Y. Zhou, H.J. Wang, T.T. Zhuang, Y. Cao, Z.Y. Yun, Q. Yu, J.H. Zhu, J. Phys. Chem. C 112 (2008) 6740.
[21] A. Taguchi, F. Schüth, Microporous Mesoporous Mater. 77 (2005) 1.
[22] A. Gedeon, A. Lassoued, J.L. Bonardet, J. Fraissard, Microporous Mesoporous Mater. 44–45 (2001) 801.
[23] S.F.J. Hackett, R.M. Brydson, M.H. Gass, I. Harvey, I.A.D. Newman, K. Wilson, A.F. Lee, Angew. Chem. 119 (2007) 8747.
[24] D.O. Zárate, F. Bouyer, H. Zschiedrich, P.J. Kooyman, P. Trens, J. Iapichella, R. Durand, C. Guillem, E. Prouzet, Chem. Mater. 20 (2008) 1410.
[25] A. Thomas, F. Goettmann, M. Antonietti, Chem. Mater. 20 (2008) 738.
[26] A. Zukal, H. Siklova, J. Cejka, Langmuir 24 (2008) 9837.
[27] Z.Y. Wu, H.J. Wang, T.T. Zhuang, L.B. Sun, Y.M. Wang, J.H. Zhu, Adv. Funct. Mater. 18 (2008) 82.
[28] J.H. Xu, T.T. Zhuang, Y. Cao, J. Yang, J.J. Wen, Z.Y. Wu, C.F. Zhou, L. Huang, Y. Wang, M.B. Yue, J.H. Zhu, Chem. Asian J. 2 (2007) 996.
[29] H.P. Boehm, Carbon 40 (2002) 145.
[30] P. Chen, X. Wu, J. Lin, K.L. Tan, Science 285 (1999) 91.
[31] H.M. Cheng, M.S. Dresselhaus, Science 287 (2000) 593.
[32] H. Suda, K.J. Haraya, J. Phys. Chem. B 101 (1997) 3988.

[33] H. Suda, K. Haraya, Chem. Commun. (1997) 93.
[34] H.C. Foley, Microporous Mater. 4 (1995) 407.
[35] F. Rodríquez-Reinoso, Carbon 36 (1998) 159.
[36] S. Flandrois, B. Simon, Carbon 37 (1999) 165.
[37] R. Ryoo, S.H. Joo, S.J. Jun, Phys. Chem. B 103 (1999) 7743.
[38] J.A. Fournier, Z.H. Luan, US Patent 0133047 A1 (2005).
[39] D. Zhao, J. Feng, Q. Huo, N. Melosh, G.H. Fredrickson, B.F. Chmelka, G.D. Stucky, Science 279 (1998) 548.
[40] S. Jun, S.H. Joo, R. Ryoo, J. Am. Chem. Soc. 122 (2000) 10712.
[41] H.Q. Wu, D.M. Xu, Q. Wang, Q.Y. Wang, G.Q. Su, X.W. Wei, J. Alloys Compd. 463 (2008) 78.
[42] S.H. Joo, S.J. Choi, I. Oh, J. Kwak, Z. Liu, O. Terasaki, R. Ryoo, Nature 412 (2001) 169.
[43] H. Sugimura, A. Hozumi, T. Kameyama, O. Takai, Adv. Mater. 13 (2001) 677.
[44] H.P. Lin, C.Y. Chang-Chien, C.Y. Tang, C.Y. Lin, Microporous Mesoporous Mater. 93 (2006) 344.
[45] E. Leontidis, Current Opin, Colloid Interf. Sci. 7 (2002) 81.
[46] C. Dicke, G. Hähner, J. Phys. Chem. B 106 (2002) 4450.
[47] M. Kruk, M. Jaroniec, Chem. Mater. 13 (2001) 3169.
[48] Y.M. Wang, Z.Y. Wu, Y.L. Wei, J.H. Zhu, Microporous Mesoporous Mater. 84 (2005) 127.
[49] A. Norman, in: D.L. Davis, M.T. Nielsen (Eds.), Tobacco Production Chemistry and Technology, Blackwell Science, London, 1999, pp. 363–369.
[50] N.Ya. Mikhailovskii, A.P. Iinitskii, A.A. Korolev, Kazan. Med. Zh. 60 (1979) 65.
[51] Y. Xu, Q. Jiang, Y. Cao, Y.L. Wei, Z.Y. Yun, J.H. Xu, Y. Wang, C.F. Zhou, L.Y. Shi, J.H. Zhu, Adv. Funct. Mater. 14 (2004) 1113.
[52] D.R. Rilison, Science 299 (2003) 1698.